DAFTAR PUSTAKA

Astuti, W. (2012). Pembuatan Nickel Pig *Iron* (NPI) dari bijih nikel laterit Indonesia. Menggunakan mini blast furnace. Prosiding INSINas, p.66-71.

Boldt, J.R. (1966). The winning of nickel its geology, mining, and extractive metallurgy, toronto.

Butt, C.R.M. (1989). Geomorphology and climatic history—keys to understanding geochemical dispersion in deeply weathered terrain, Ontario Geological Survey, Volume 3, pp. 323-334

Butt, C.R.M., and Zeegers, H. (1992). Regolith exploration geochemistry in tropical and subtropical terrains. handbook of exploration geochemistry, 4. Elsevier, Amsterdam, pp. 607

Brand, N.W., Butt, C.,R.,M., and Elias, M. (1998). Nickel laterites: classification and features AGSO Journal of Australian Geology & Geophysics, 17 (4), 81-88.

Cao, Y., Sun Y., Gao, P., Han, Y., and Li, Y. (2021). Mechanism for suspension magnetization roasting of *Iron* ore using straw-type biomass reductant. International Journal of Mining Science and Technology.

Cao, Z.C., Sun, T.C., Yang, H.F., Wang, J.J., Wu, X.D. (2010). Perolehan of *Iron* and nickel from nickel laterite ore by direct reduction roasting and *Magnetic Separation*. J. Univ. Sci. Technol. Beijing 32 (6), pp. 708–712

Carvalho-e-Silva, M. L., dkk., (2003). Incorporation of Ni into natural *goethite*: An investigation by X-ray absorption spectroscopy, American Mineralogist, 88, 876–882

Chen. Y., Guo, Z., Wang, X., Qiu, C. (2007). Sample preparation Journal of Chromatography A, 1184 (2008) 191–219

Choi Y., Lee I., and Moon I. (2021). Geochemical and mineralogical characteristics of *garnierite* from the Morowali Ni-laterite deposit in Sulawesi, Indonesia. Frontiers in Earth Science, Volume 9

Dalvi, A.D., Bacon, W.G., & Osborne, R. (2004). The past and the future of nickel laterites. In: PDAC 2004 International Convention. Trade Show & Investors Exchange, North Carolina, USA, pp. 1-27

Elias, M. (2002). Nickel laterite deposits: Geological overview, resources and exploitation, giant ore deposits: characteristics, genesis, and exploration. CODES Special Publication., Volume 4, pp.205-220.

Ezhov, A.M., Shvaljov, Y.B. (2015). Dry *magnetic separation* of *iron* ore of the bakchar posit., Procedia Chemistry., Volume 15., pp.160-166.

, dkk., (2015). Microwave carbothermic reduction roasting of a low grade ckeliferous silicate laterite ore. Minerals Engineering, pp. 1-10.

Freyssinet, P., and Itard, Y. (1997). Gold signal in various weathering conditions: Application to exploration

Ginting, I., dan Sufiandi, D. (2015). Percobaan peningkatan kadar mangan menggunakan magnetic separator. Pusat Penelitian Metalurgi

Haya, A., Wawan, A.C, dan Firman. (2019). Penyebaran endapan nikel laterit Pulau Obi Kabupaten Halmahera Selatan Provinsi Maluku Utara. Journal of Science and Engineering, Volume 1, pp. 25-33

Kawahara, M., (1988). Reducibility of laterite ore. Metallurgical Transaction B. 19B 181 – 186.

Kim, J., Dodbiba, G., Tanno, H., Okaya, K., Matsuo, S., Fujita, T. (2010). Calcinations of low-grade laterite for concentration of Ni by *Magnetic Separation*. Miner. Eng. 23 (4), pp. 282–288.

Kose, S. (2010). Hydrometallurgical Processing of Lateritical Nickel Ores. Thesis: Metallurgical and Materials Engeneering, 195.

Kyle, J. (2010). Nickel Laterit Processing Technologies-Where to Next. Murdoch University: Repository

Li, G.H., Shi, T.M., Rao, M.J., Kiang, T., Zhang, Y.B. (2012). Beneficiation of nickeliferous laterite by reduction roasting in the presence of sodium sulfate. Miner. Eng. 32, pp. 19–26

Lubbe, S., Munsami, R., Fourie, D. (2012). Beneficiation of zircon sand in South Africa, J S AFR I MIN METALL, 112 pp. 583 – 588

Moskalyk, R.R., Alfantazi, A.M. (2002). Nickel laterite processing and electrowinning practice. Miner. Eng, Volume 15, pp. 593–605.

Mudd, G. (2010). Global trends and issues in nickel mining: sulfides versus laterites. Ore Geol, Volume 38, pp. 9–26.

Nurhakim., Dwiatmoko, M.U., Romla, N.H., Adip, M. (2011). Identifikasi potensi endapan bijih besi laterit di Tengah Pulau Sebuku, Provinsi Kalimantan Selatan., Jurnal Info Teknik, Volume 12 No. 2. pp.48-53.

Rhamdhani, M.A., Hayes, P.C., Jak, E. (2009). Nickel laterite Part 1 – microstructure and phase characterizations during reduction roasting and leaching. Miner. Process. Extr. Metall. Rev. 3., Vol. (118), pp. 129– 145

Robertson, I.D.M., and Butt, C.RM. (1993). Atlas of weathered rocks. CSIRO Australia, Exploration Geoscience, Volume 390, p. 32

Santoso, A., Marzuki, A.R., Afrida, Y. (2022). Analisis kehandalan kinerja magnet parator terhadap material logam yang bersifat feromagnetik di PT. Bukit Asam ɔk, Unit Pelabuhan Tarahan. Jurnal Ilmiah Teknik Elektro UML (JITRO-ML), 5(1), 34-40

Seisfelnassr, A.A.S., Moslim, E.M and Abouzeid, A.Z.M. (2012). Effective processing of law-grade *iron* of throgh gravity and *magnetic separation* techniques. Phisicochemical Problem of Mineral Processing 48(2):pp. 567-578.

Setiawan, IF., Prabowo, H. (2021). Analisis pengaruh pemberian cangkang kemiri terhadap nilai parameter batubara di CV. Bara Mitra Kencana, Kota Sawahlunto, Sumatera Barat Jurnal Bina Tambang, Vol. 6 , No. 1

Solar, M.Y., Mostaghel, S. (2015). Smelting of difficult laterite ores. Institute of Materials, Minerals and Mining and The AusIMM. Volume 124. Nomor 1.

Subagja, R. (2016). Peningkatan kadar nikel dalam laterit jenis limonit dengan cara peletasi, pemanggangan reduksi dan pemisahan magnet campuran bijih, batu bara, dan Na_2SO_4. Pusat Penelitian Metalurgi dan Material. Tanggerang Selatan pp. 103-115.

Sukandarrumidi, (2007). Geologi mineral logam, Gadjah Mada University Press. Yogyakarta.

Svoboda, J. (2004). Magnetic techniques for the treatment materials. Kluwer Academic Publisher. New york, p.78.

Tonggiroh, A, Mustafa M, Suharto, (2012). Analisis pelapukan serpentin dan endapan nikel laterit daerah Pallangga Kabupaten Konawe Selatan Sulawesi Tenggara.

Usachyov, P.A., and Korytny, S.Y. (1998). Magnetic-gravity separation of *iron* ore. Indian Jurnal of Enginering and Materials Science, Volume 5, pp.130-135.

Wang Z.H., Chu M.S., Liu Z.G., Wang H., Zhao W., Gao L.H. (2017). Preparing ferro-nickel alloy from low-grade laterite nickel ore based on metallized reduction-*Magnetic Separation*. Metals, 313, pp. 1–4

Wills, B., dan Finch 3.A. (2006). Mineral processing technology an introduction to the practical aspects of ore treatment and mineral perolehan. New York: Pergamon Press, p.550.

Wills, B.A dan Napier, M.T, (2005). Magnetic and electrical separation Wills. Mineral Processing Technology (Elsevier), 353–72

Zhu, D.Q., Cui, Y., Vining, K., Hapugoda, S., Douglas, J., Pan, J., Zheng, G.L. (2012). Upgrading low nickel content laterite ores using selective reduction followed by *Magnetic Separation*. Int. J. Miner. Process. 106–109, 1–7

Zhu, D.Q., Pan L.T., Guo Z.Q., Pan J., Zhang, F. (2019). Utilization of limonitic nickel laterite to produce ferronickel concentrate by the selective reduction-*Magnetic Separation* process. Adv Powder Technol, 30 pp. 451–60.

LAMPIRAN

Lampiran 1
Hasil Analisis *X-Ray Diffraction* (XRD)

HASIL ANALISIS *X-RAY DIFFRACTION* (XRD) SAMPEL AWAL

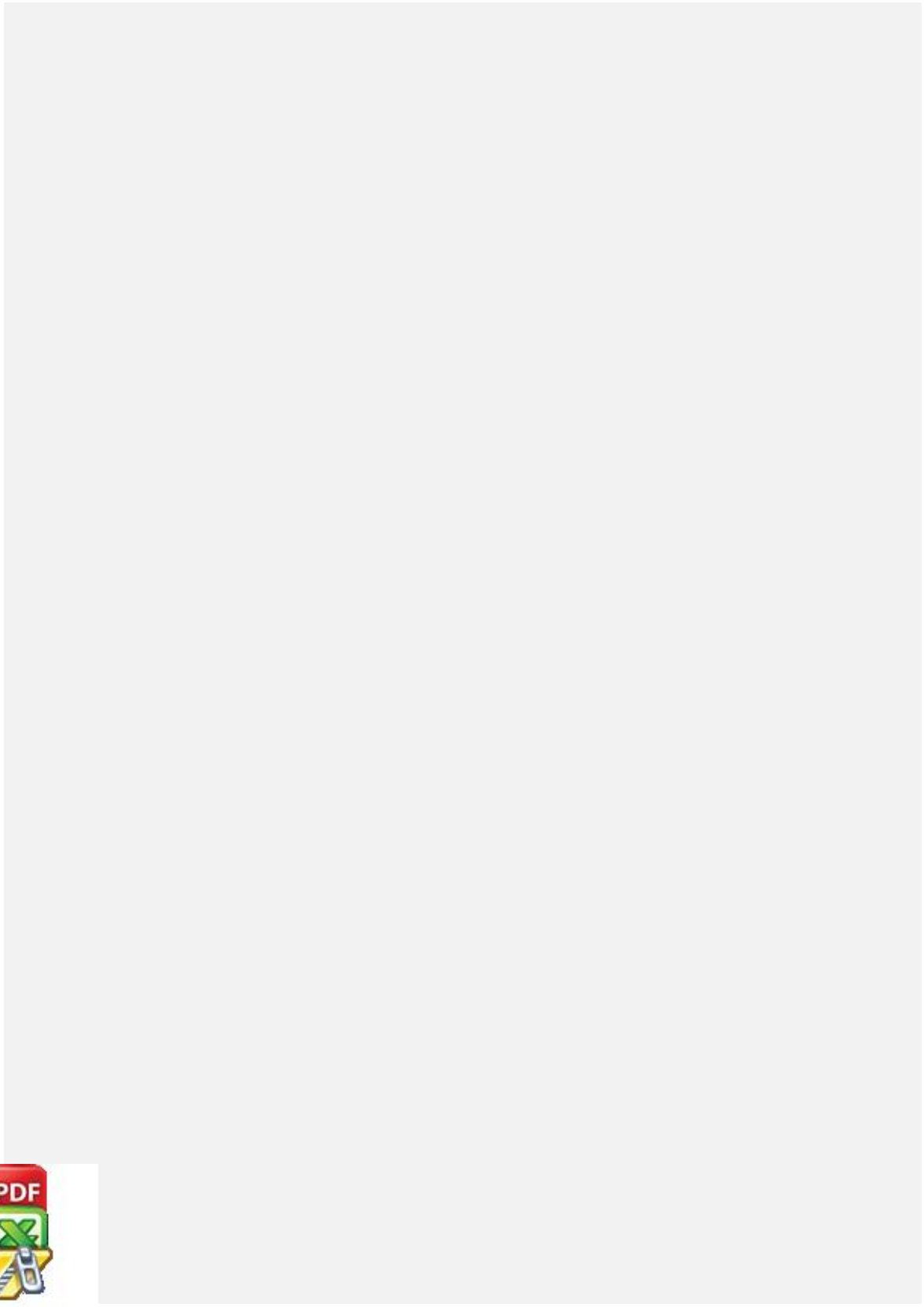

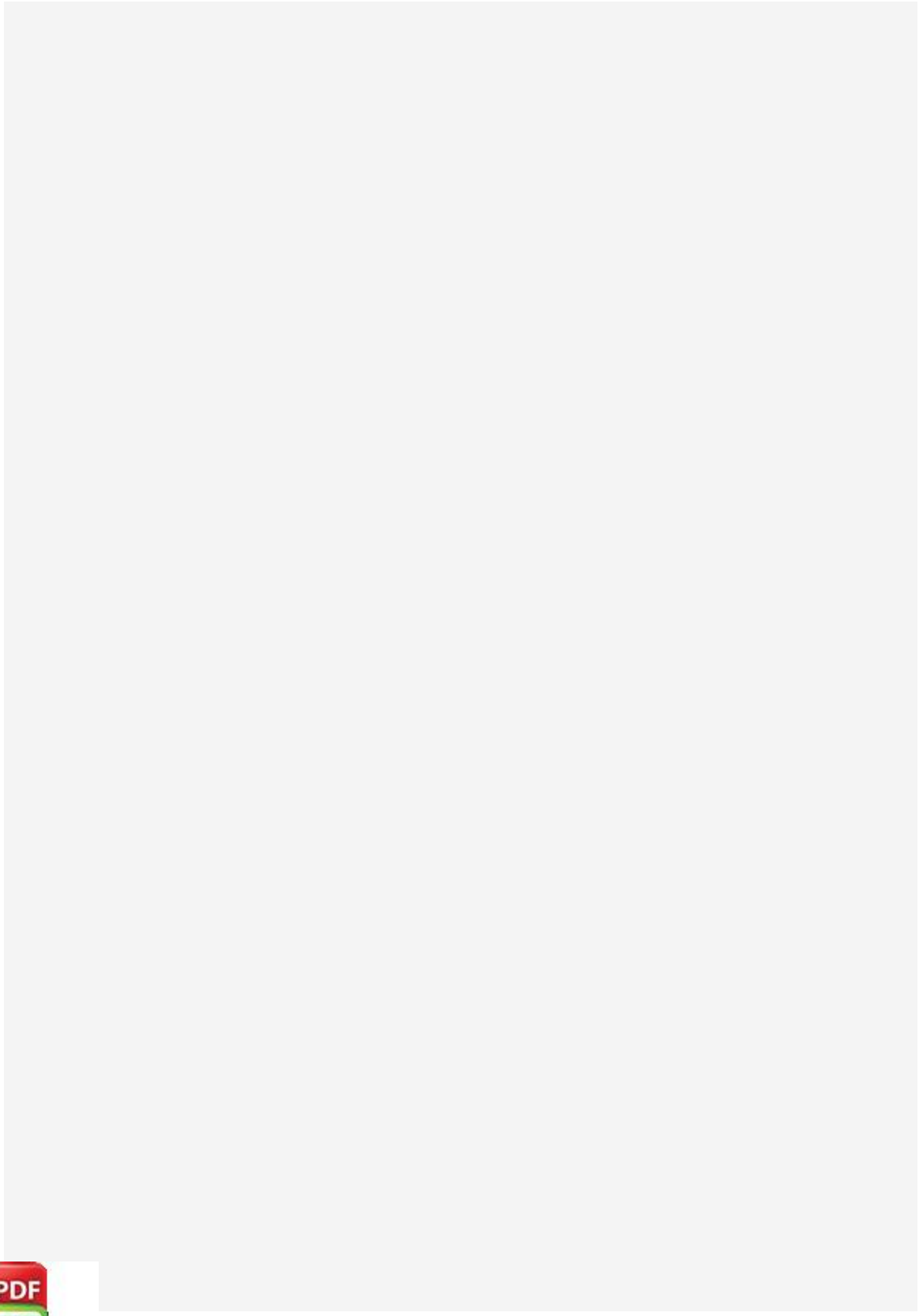

HASIL ANALISIS *X-RAY DIFFRACTION* (XRD) SAMPEL P -177+149

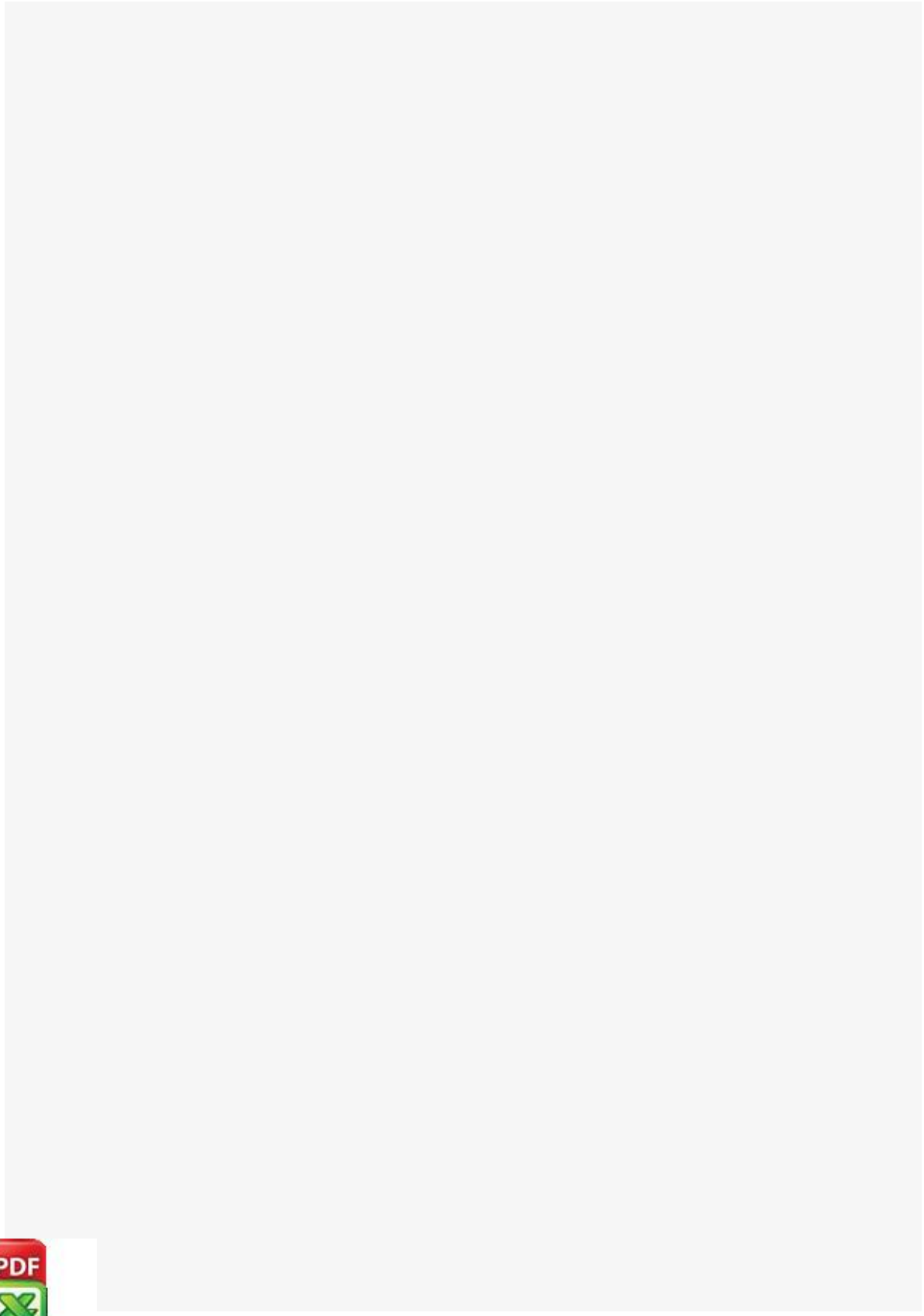

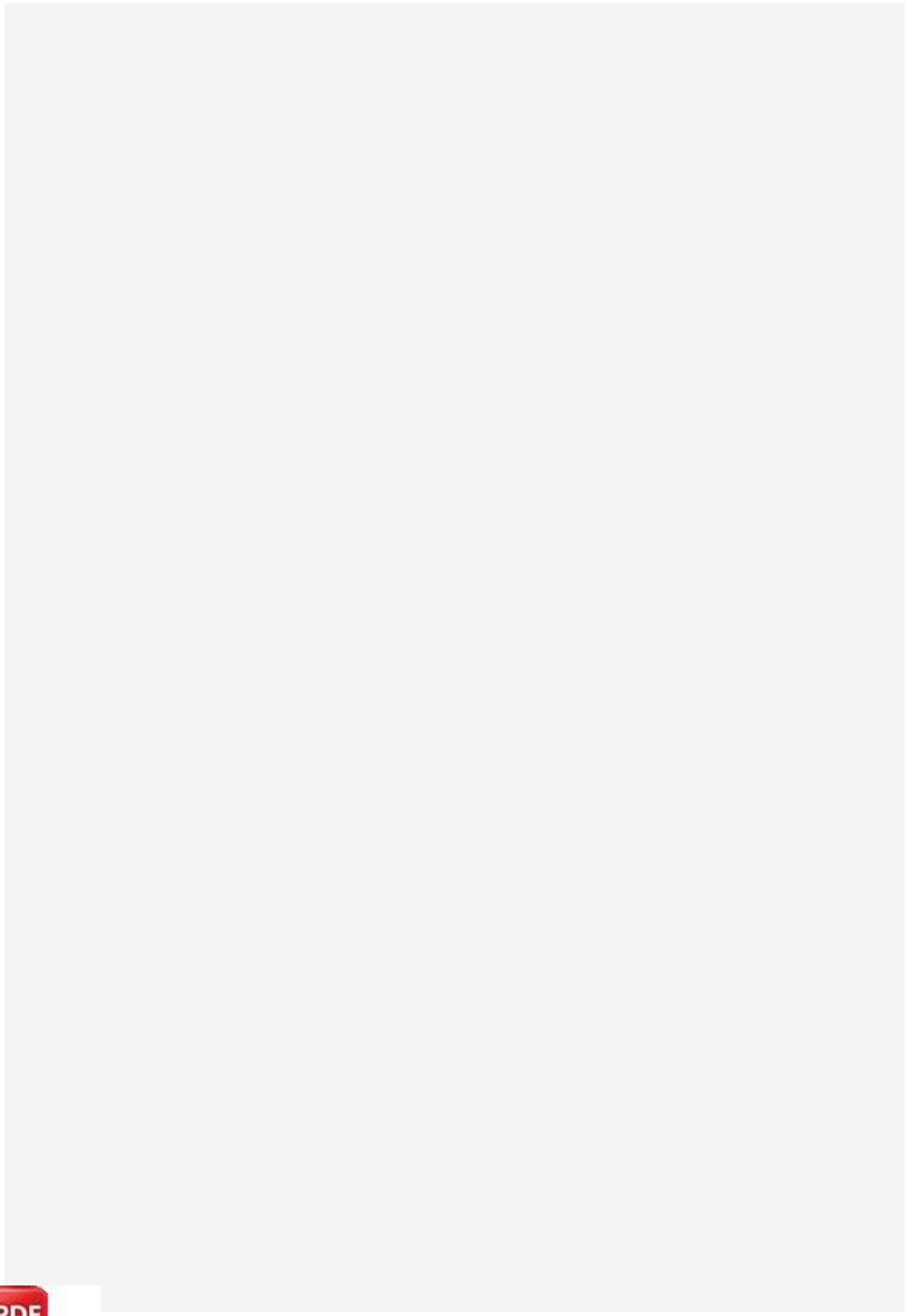


PDF
Optimized using
trial version
www.balesio.com

HASIL ANALISIS *X-RAY DIFFRACTION* (XRD) SAMPEL P -149+105

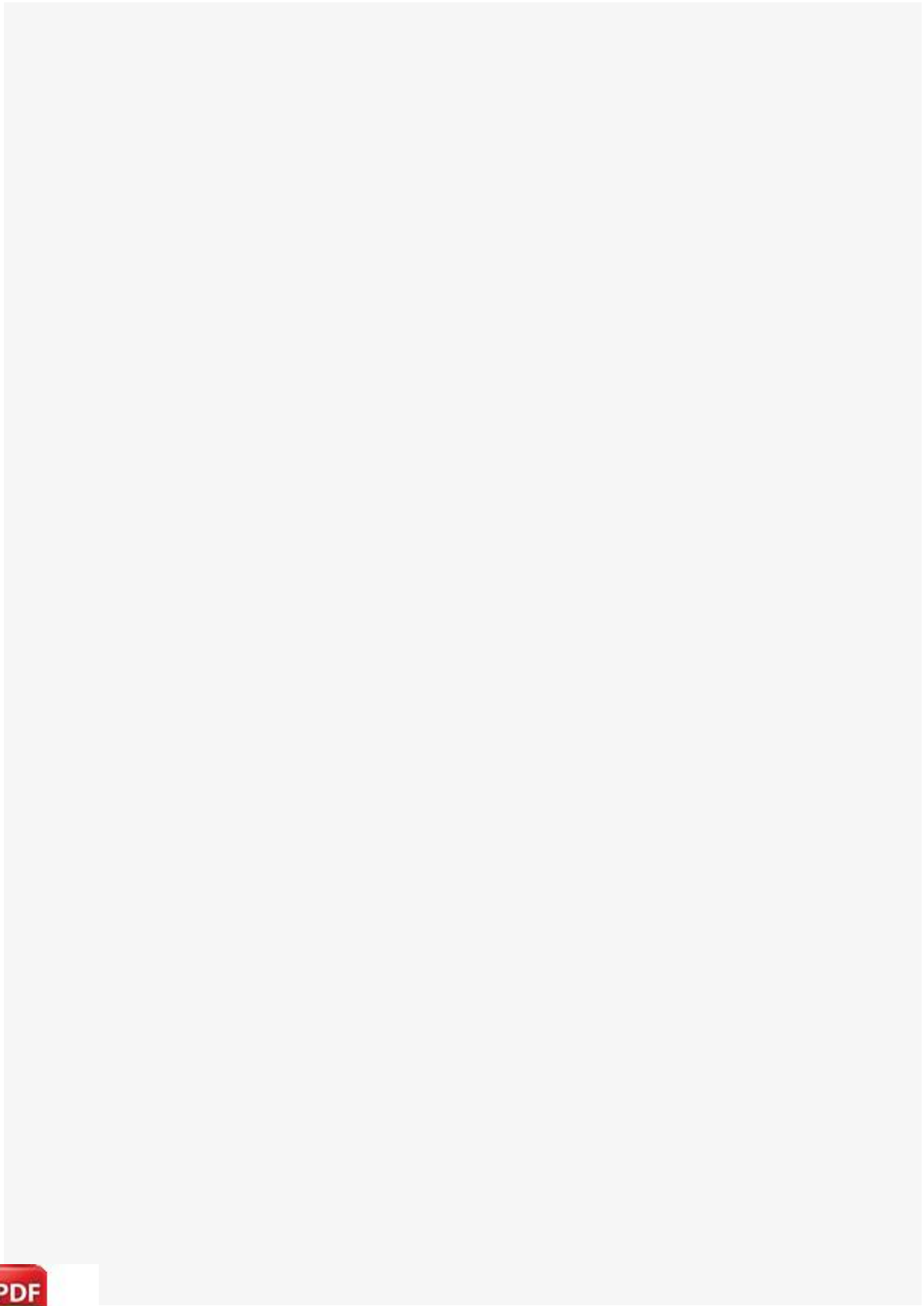

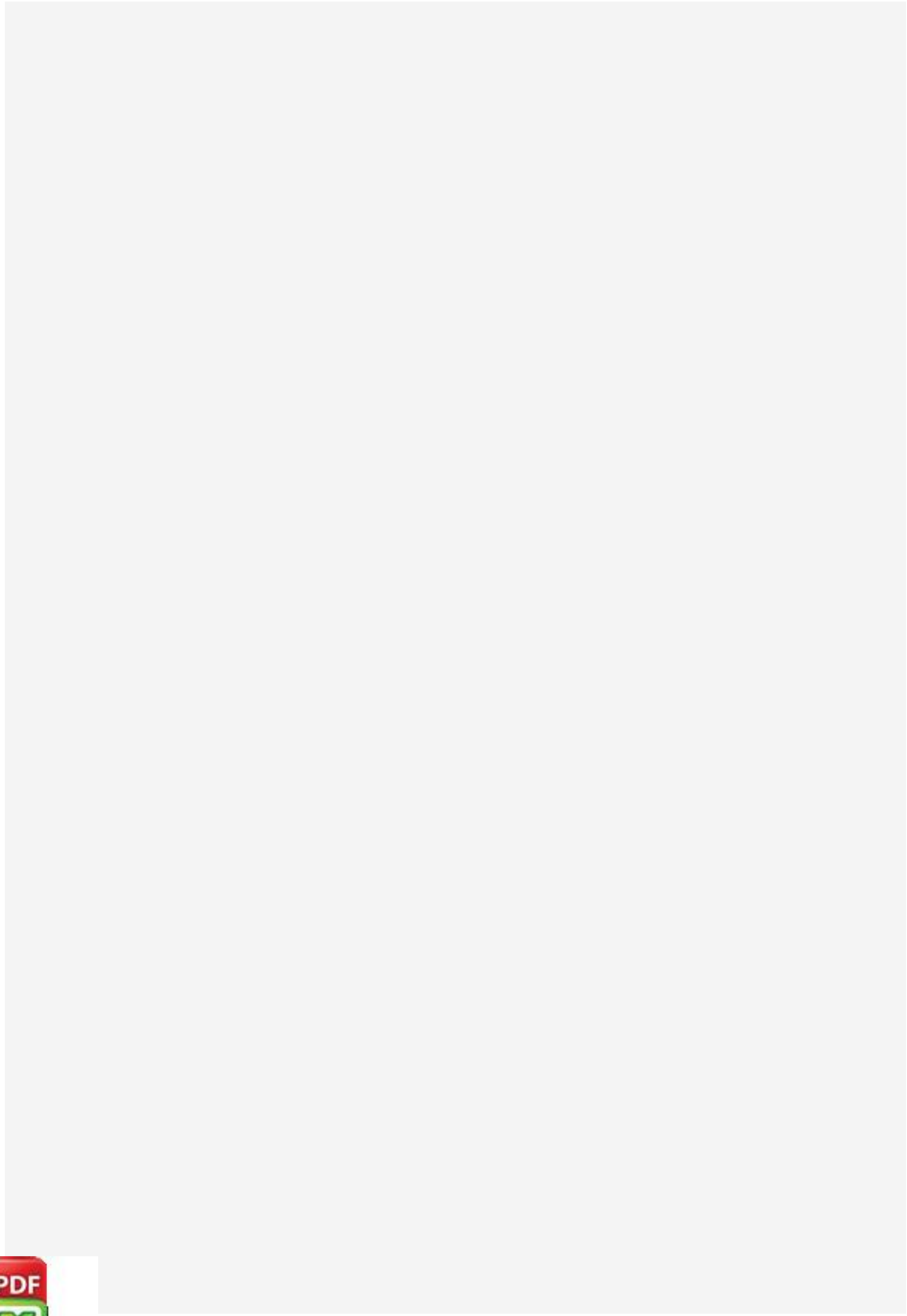


PDF
Optimized using
trial version
www.balesio.com

HASIL ANALISIS *X-RAY DIFFRACTION* (XRD) SAMPEL P -105+74

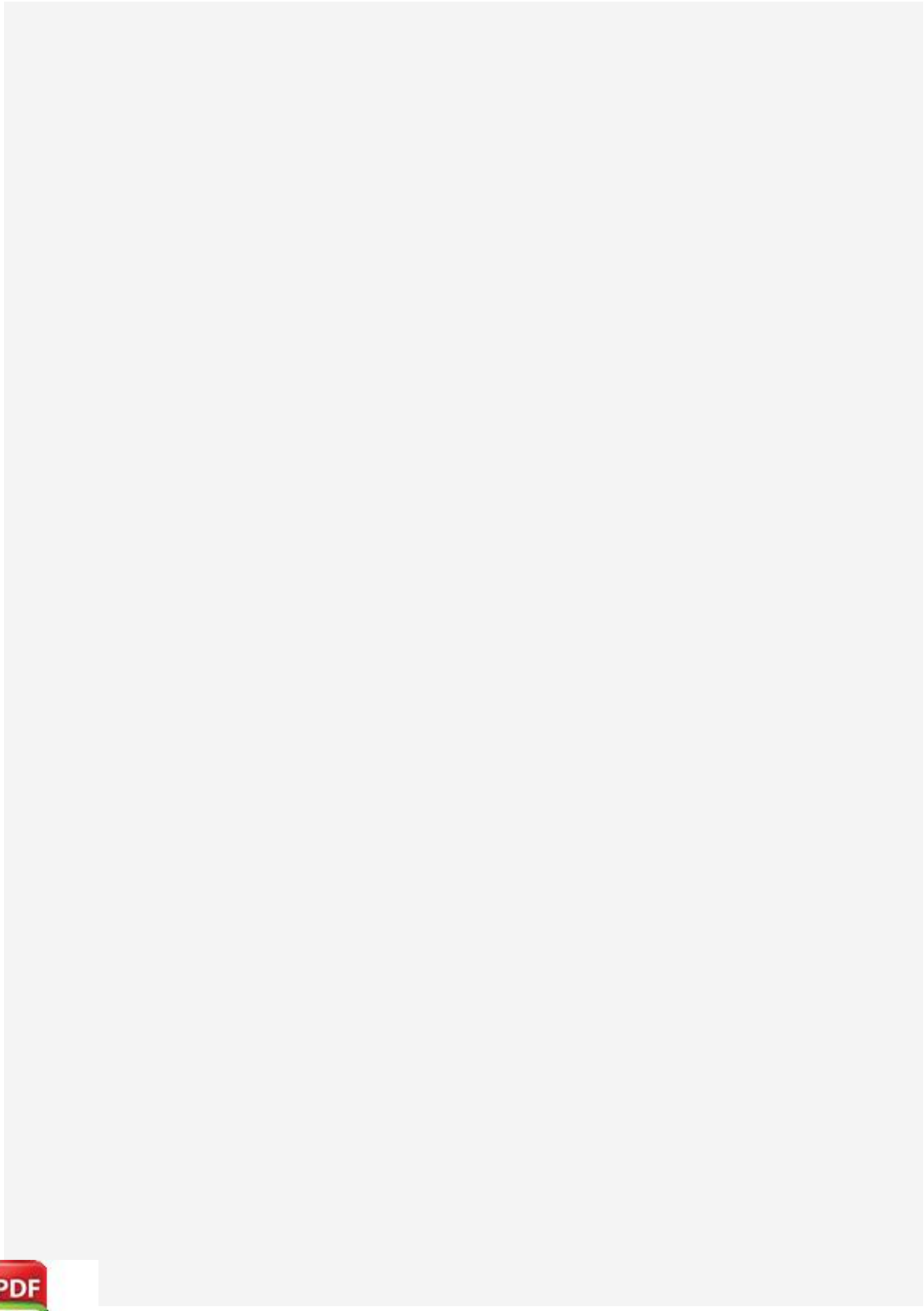


PDF
Optimized using
trial version
www.balesio.com


PDF
Optimized using
trial version
www.balesio.com

HASIL ANALISIS *X-RAY DIFFRACTION* (XRD) SAMPEL P -74


PDF
Optimized using
trial version
www.balesio.com

HASIL ANALISIS *X-RAY DIFFRACTION* (XRD) SAMPEL TP -177+149


PDF
Optimized using
trial version
www.balesio.com

HASIL ANALISIS *X-RAY DIFFRACTION* (XRD) SAMPEL TP -149+105

HASIL ANALISIS *X-RAY DIFFRACTION* (XRD) SAMPEL TP -105+74

Match! Phase Analysis Report

Sample: NMD-TP-140 (5-70)

Sample Data

File name	NMD-TP-140.RAW
File path	D:/naufal/UNHAS/Skripsi/Skripsi/Data XRD Sampel Akhir/Naufal/NMD-TP-140
Data collected	Feb 2, 2024 13:13:21
Data range	5.000° - 70.000°
Original data range	5.000° - 70.000°
Number of points	3251
Step size	0.020
Rietveld refinement converged	No
Alpha2 subtracted	No
Background subtr.	No
Data smoothed	Yes
Radiation	X-rays
Wavelength	1.540600 Å

Analysis Results

Phase composition (Weight %)

Elemental composition (Weight %)

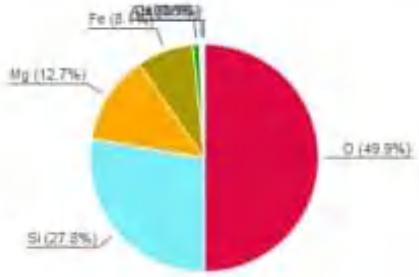

Index	*Amount (%)*	*Name*	*Formula sum*
A	30.6	Lizardite	Al0.22 Fe0.15 H4 Mg2.79 O9 Si1.84
B	28.8	Silicon oxide Quartz low	O2 Si
C	27.8	Talc	H2 Mg3 O12 Si4
D	11.3	Goethite	Fe O2
E	1.8	Montmorillonite	Al2 Ca0.5 O12 Si4
	12.0	*Unidentified peak area*	

Amounts calculated by RIR (Reference Intensity Ratio) method

Element	*Amount (weight %)*
O	49.9%(*)
Mg	12.7%
Fe	8.1%
Al	0.9%
Ca	0.1%
**LE (sum)*	*50.5%*

Details of identified phases

A: Lizardite (30.6 %)

Formula sum	Al0.22 Fe0.15 H4 Mg2.79 O9 Si1.84
Entry number	96-900-4995
Figure-of-Merit (FoM)	0.000000
Total number of peaks	111
Peaks in range	27
Peaks matched	6
Intensity scale factor	0.47
Space group	P 3 1 m
Crystal system	trigonal (hexagonal axes)
Unit cell	*a*= 5.3160 Å *c*= 7.1500 Å
I/Ic	1.38
Calc. density	2.674 g/cm³
Reference	Mellini M., Zanazzi P. F., "Effects of pressure on the structure of lizardite-1TSample: at P = 12.5 kbar", European Journal of Mineralogy **1**, 13-19 (1989)

B: Silicon oxide Quartz low (28.8 %)*

Formula sum	O2 Si
Entry number	96-101-1160
Figure-of-Merit (FoM)	0.789206*
Total number of peaks	70
Peaks in range	18
Peaks matched	10
Intensity scale factor	0.96
2theta correction	-0.016°
Space group	P 32 2 1 S
Crystal system	trigonal (hexagonal axes)
Unit cell	a= 4.9100 Å c= 5.4000 Å
I/Ic	3.01
Meas. density	2.660 g/cm³
Calc. density	2.654 g/cm³
Reference	Machatschki F, "Kristallstruktur von Tiefquarz", Fortschritte der Mineralogie **20**, 45-47 (1936)

C: Talc (27.6 %)

Formula sum	H2 Mg3 O12 Si4
Entry number	96-900-8298
Figure-of-Merit (FoM)	0.000000
Total number of peaks	251
Peaks in range	183
Peaks matched	65
Intensity scale factor	0.32
Space group	C -1
Crystal system	triclinic (anorthic)
Unit cell	a= 5.2900 Å b= 9.1730 Å c= 9.4600 Å α= 90.460° β= 98.680 ° γ= 90.090 °
I/Ic	1.03
Calc. density	2.776 g/cm³
Reference	Perdikatsis B., Burzlaff H., "Strukturverfeinerung am talk Mg3[(OH)2Si4O10]", Zeitschrift fur Kristallographie **156**, 177-186 (1981)

D: Goethite (11.3 %)*

Formula sum	Fe O2
Entry number	96-901-5697
Figure-of-Merit (FoM)	0.654345*
Total number of peaks	187
Peaks in range	37
Peaks matched	14
Intensity scale factor	0.40
2theta correction	0.058°
Space group	P b n m
Crystal system	orthorhombic
Unit cell	a= 4.6188 Å b= 9.9528 Å c= 3.0236 Å
I/Ic	3.17
Calc. density	4.198 g/cm³
Reference	Hazemann J.-L., Bérar J. F., Manceau A., "Rietveld studies of the aluminium-iron substitution in synthetic goethite", Materials Science Forum **79-82**, 821-826 (1991)

E: Montmorillonite (1.8 %)

Formula sum	Al2 Ca0.5 O12 Si4
Entry number	96-900-2780
Figure-of-Merit (FoM)	0.000000
Total number of peaks	92
Peaks in range	92
Peaks matched	30
Intensity scale factor	0.36
Space group	P 1
Crystal system	triclinic (anorthic)
Unit cell	a= 5.1800 Å b= 8.9800 Å c= 15.0000 Å α= 90.000° β= 90.000 ° γ= 90.000 °
I/Ic	17.33
Calc. density	1.801 g/cm³
Reference	Viani A., Gualtieri A., Artioli G., "The nature of disorder in montmorillonite by simulation of X-ray powderpatterns Note: Structural simulation model", American Mineralogist **87**, 966-975 (2002)

(*)2theta values have been shifted internally for the calculation of the amounts, the intensity scaling factors as well as the figure-of-merit (FoM), due to the active search-match option 'Automatic zero point adaption'.

Candidates

Name	Formula	Entry No.	FoM
MOL-3CdS	C158 H138 Cd17 N4 S32	96-411-1893	0.7016
	C12 Ga O5	96-770-3817	0.6938
	Cs4 H62 K7 Na5 Nb23 O108 V5	96-712-7393	0.6886
	C10 H10 Co3 F2 N2 O8 P2	96-431-0851	0.6865
	Sc	96-151-2540	0.6801
	Be F2	96-153-1932	0.6786
	C114 Mn N7 O74 Si2 W18	96-711-6609	0.6714

Portlandite (deuterated)	Ca D2 O2	96-901-0908	0.6677
Lithium Cobalt Oxide	Co Li0.58 O2	96-155-0394	0.6672
	C116 Cl4 Fe N7 O72 Si2 W18	96-711-6607	0.6667
Li0.16 (Ni0.7 Fe0.15 Co0.15)1.03 O2	Co0.1545 Fe0.1545 Li0.16 Ni0.721 O2	96-152-6297	0.6631
Sodium tetraproply uranyl peroxide	C1.66 H3.6 N0.14 Na0.17 O1.68 U0.31	96-410-5386	0.6628
Si O2	O2 Si	96-153-8065	0.6588
	C8 H136 Fe6 N4 Na14 O184 Se6 W34	96-711-5857	0.6565
Rb3GaF6	F6 Ga Rb3	96-771-3195	0.6562
	O45 P9 V12	96-400-1392	0.6536
	C4 N5 S3	96-411-6670	0.6521
Lithium Cobalt Oxide	Co Li0.5 O2	96-155-0393	0.6476
Birnessite	H4 Mn Na0.29 O2.691	96-901-0156	0.6434
Li0.08 (Ni0.7 Fe0.15 Co0.15)1.03 O2	Co0.1545 Fe0.1545 Li0.08 Ni0.721 O2	96-152-6299	0.6430
	C116 Ag2 Cr Lu2 Mn4 N14 O78 Si2 W18	96-712-0260	0.6427
Zippeite	H27 Na5 O52 S4 U8	96-900-4756	0.6403
Na0.364 Mn O2 (H2 O)0.544	H1.088 Mn Na0.364 O2.544	96-153-1680	0.6400
Brucite	H2 Mg O2	96-900-2352	0.6370
	Cs4 H74 K8 Na5 Nb23 O115 V6	96-712-7394	0.6364
COV-3CdS-BPy	C166 H138 Cd17 N2 S30	96-410-0573	0.6346
	Hg Zr	96-152-2700	0.6335
beryllium bis(hypophosphite)	Be H4 O4 P2	96-201-4099	0.6321
(C (N H2)3)18 (Na (U O2)3 (O H) (H2 O)6 (As4 W40 O140 (W O))) (H2 O)25	C12.05 As4 N35.95 Na O179 U3 W41	96-153-6613	0.6312
Rb2 Sb8 S13 (H2 O)3.28	H6.56 O3.28 Rb2 S13 Sb8	96-152-6921	0.6303
	Ba Pb Zn	96-152-7803	0.6298
	Cu F H4 O5 P	96-154-5244	0.6265
	As2 Cd O6	96-220-0092	0.6254
	As2 Cd O6	96-900-7894	0.6254
Rb (Hg F3)	F3 Hg Rb	96-152-7535	0.6249
(Eu Yb)	Eu Yb	96-152-4623	0.6234
cis-Diaqua-(2,2-bipyridyl-N,N')-copper sulfate	C10 H12 Cu N2 O6 S	96-210-2510	0.6213
	Cs4 Se4 Si	96-810-1314	0.6209
Ho Ni C2	C2 Ho Ni	96-154-0779	0.6206
(P Cl4)3 (Ti Cl6) (P Cl6)	Cl24 P4 Ti	96-153-0749	0.6201
Ba Ga Sn D	Ba D Ga Sn	96-412-4017	0.6199
K (I O3)	I K O3	96-154-1797	0.6188
Zippeite	H2 N4 O21 S2 U4	96-900-4757	0.6181
Volborthite	Cu3 H6 O11 V2	96-901-4305	0.6173
	Nb Rh	96-231-0203	0.6115
Rb Ca F3	Ca F3 Rb	96-153-0113	0.6102
	C128 N8 O74 Si2 W20 Zn4	96-431-6561	0.6099
	Ca O2	96-153-0293	0.6095
Lithium Cobalt Oxide	Co Li0.42 O2	96-155-0391	0.6084
Pb0.855 ((U O2)4 O2.710 (O H)4.290) (H2 O)4	H12.29 O19 Pb0.855 U4	96-152-1509	0.6074
(Sn Cl (H2 O)2) (Sn Cl3) (H2 O)	Cl4 H6 O3 Sn2	96-153-4642	0.6052
Thallium tridecafluorotetraantimonate(III)	F13 Sb4 Tl	96-156-7935	0.6050
and 22 others...			

Search-Match

Settings

Reference database used	COD-Inorg 2023.12.05
Automatic zeropoint adaptation	Yes
Downgrade entries with low scaling factors	Yes
Minimum figure-of-merit (FoM)	0.60
2theta window for peak corr.	0.30 deg.
Minimum rel. int. for peak corr.	0
Parameter/influence 2theta	0.50
Parameter/influence intensities	0.50
Parameter multiple/single phase(s)	0.50

Criteria for entries added by user

Reference:

Entry number: 96-901-5697;96-900-4995;96-900-8298;96-900-2780

Peak List

No.	*2theta [°]*	*d [Å]*	*I/I0 (peak height)*	*Counts (peak area)*	*FWHM*	*Matched*
1	5.66	15.6017	349.51	32.85	0.6400	E
2	6.70	13.1821	103.83	4.27	0.2800	
3	9.32	9.4815	66.79	6.37	0.6493	C
4	12.38	7.1439	368.27	19.47	0.3600	A
5	18.66	4.7514	286.95	20.23	0.4800	
6	19.70	4.5029	246.43	27.50	0.7600	C,E
	0.98	4.2309	461.87	67.82	1.0000	B,D
	4.92	3.5702	376.28	24.31	0.4400	A

12	31.14	2.8698	262.91	15.44	0.4000	E
13	33.16	2.6995	187.96	8.83	0.3200	D
14	34.74	2.5802	253.08	29.73	0.8000	C,D,E
15	35.68	2.5144	339.53	55.84	1.1200	C,D,E
16	36.58	2.4545	485.36	45.61	0.6400	B,C,D,E
17	37.36	2.4051	102.53	10.84	0.7200	C
18	39.56	2.2762	130.96	13.08	0.6800	B,C
19	40.38	2.2319	117.48	15.87	0.9200	B,C,E
20	42.44	2.1282	84.01	4.38	0.3554	A,B,C,E
21	45.04	2.0112	103.72	3.66	0.2400	D
22	50.22	1.8152	162.44	7.63	0.3200	B,C
23	52.94	1.7282	176.04	8.27	0.3200	C,E
24	53.34	1.7162	198.67	10.50	0.3600	C,D
25	53.62	1.7079	120.15	29.64	1.6800	C
26	58.90	1.5667	119.44	19.64	1.1200	A,C,D,E
27	60.00	1.5406	104.93	7.47	0.4847	A,B,C,E
28	60.90	1.5200	135.01	11.10	0.5600	C,D,E
29	61.28	1.5115	135.04	22.21	1.1200	C,D
30	63.36	1.4668	111.24	5.23	0.3200	C,D,E
31	68.30	1.3722	101.65	8.36	0.5600	B,C,D

Integrated Profile Areas

Based on calculated profile

Profile area	*Counts*	*Amount*
Overall diffraction profile	84625	100.00%
Background radiation	52647	62.21%
Diffraction peaks	31978	37.79%
Peak area belonging to selected phases	21798	25.76%
Peak area of phase A (Talc)	*5989*	*7.08%*
Peak area of phase B (Silicon oxide Quartz low)	*4447*	*5.26%*
Peak area of phase C (Montmorillonite)	*1518*	*1.79%*
Peak area of phase D (Lizardite)	*4592*	*5.43%*
Peak area of phase E (Goethite)	*5251*	*6.21%*
Unidentified peak area	10180	12.03%

Peak Residuals

Peak data	*Counts*	*Amount*
Overall peak intensity	616	100.00%
Peak intensity belonging to selected phases	458	74.33%
Unidentified peak intensity	158	25.67%

Diffraction Pattern Graphics

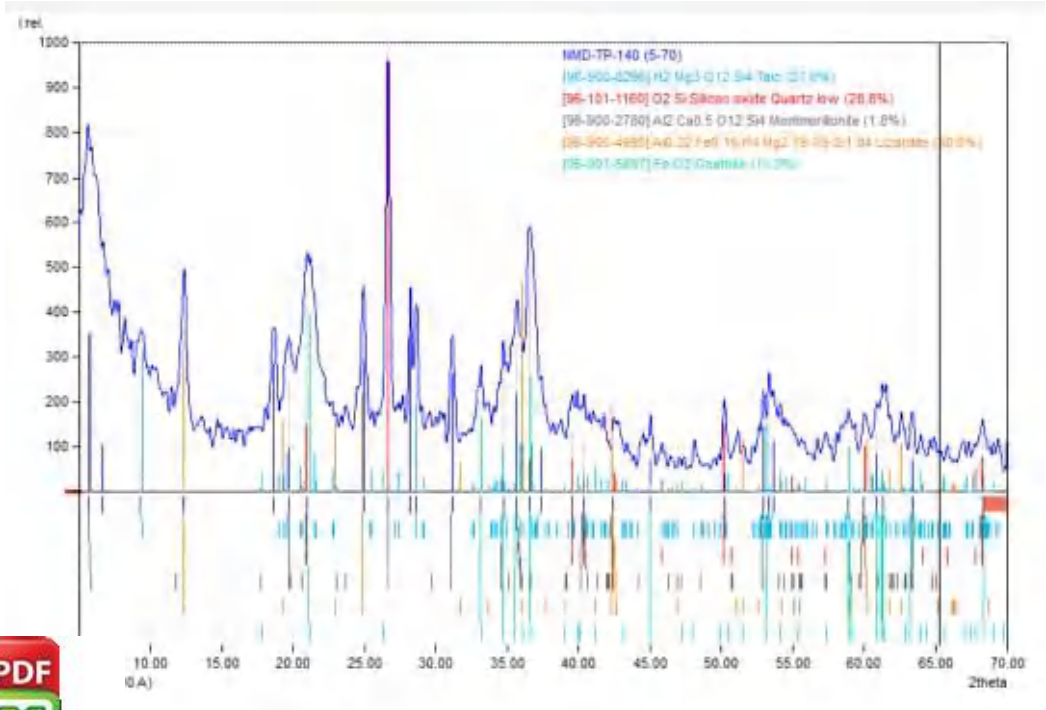

HASIL ANALISIS *X-RAY DIFFRACTION* (XRD) SAMPEL TP -74

Match! Phase Analysis Report

Sample: NMD-TP-200 (5-70)

Sample Data

File name	NMD-TP-200.RAW
File path	D:\naufal\UNHAS\Skripsi\Skripsi\Data XRD Sampel Akhir\Naufal\NMD-TP-200
Data collected	Feb 2, 2024 13:13:21
Data range	5.190° - 70.190°
Original data range	5.000° - 70.000°
Number of points	3251
Step size	0.020
Rietveld refinement converged	No
Alpha2 subtracted	No
Background subtr.	No
Data smoothed	Yes
2theta correction	0.19°
Radiation	X-rays
Wavelength	1.540600 Å

Analysis Results

Phase composition (Weight %)

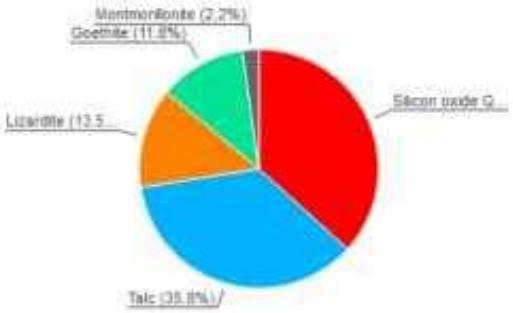

Elemental composition (Weight %)

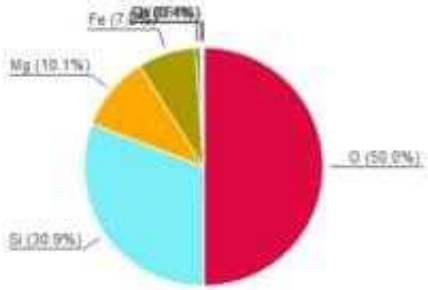

Index	*Amount (%)*	*Name*	*Formula sum*
A	36.7	Silicon oxide Quartz low	O2 Si
B	35.8	Talc	H2 Mg3 O12 Si4
C	13.5	Lizardite	Al0.22 Fe0.15 H4 Mg2.78 O9 Si1.84
D	11.8	Goethite	Fe O2
E	2.2	Montmorillonite	Al2 Ca0.5 O12 Si4
	15.0	*Unidentified peak area*	

Element	*Amount (weight %)*
O	50.0%(*)
Si	30.9%
Mg	10.1%
Fe	7.9%
Al	0.8%
Ca	0.1%
LE (sum)	50.4%

Amounts calculated by RIR (Reference Intensity Ratio) method

Details of identified phases

A: Silicon oxide Quartz low (36.7 %)*

Formula sum	O2 Si
Entry number	96-101-1160
Figure-of-Merit (FoM)	0.757052*
Total number of peaks	70
Peaks in range	18
Peaks matched	10
Intensity scale factor	0.96
2theta correction	-0.188°
Space group	P 32 2 1 S trigonal (hexagonal axes) a= 4.9100 Å c= 5.4000 Å 3.01

Meas. density	2.660 g/cm³
Calc. density	2.654 g/cm³
Reference	Machatschki F, "Kristallstruktur von Tiefquarz", Fortschritte der Mineralogie **20**, 45-47 (1936)

B: Talc (35.8 %)

Formula sum	H2 Mg3 O12 Si4
Entry number	96-900-8298
Figure-of-Merit (FoM)	0.000000
Total number of peaks	251
Peaks in range	184
Peaks matched	68
Intensity scale factor	0.32
Space group	C -1
Crystal system	triclinic (anorthic)
Unit cell	a= 5.2900 Å b= 9.1730 Å c= 9.4600 Å α= 90.460° β= 98.680 ° γ= 90.090 °
I/Ic	1.03
Calc. density	2.776 g/cm³
Reference	Perdikatsis B., Burzlaff H., "Strukturverfeinerung am talk Mg3[(OH)2Si4O10]", Zeitschrift fur Kristallographie **156**, 177-186 (1981)

C: Lizardite (13.5 %)*

Formula sum	Al0.22 Fe0.15 H4 Mg2.79 O9 Si1.84
Entry number	96-900-4995
Figure-of-Merit (FoM)	0.586259*
Total number of peaks	111
Peaks in range	28
Peaks matched	9
Intensity scale factor	0.16
2theta correction	-0.051°
Space group	P 3 1 m
Crystal system	trigonal (hexagonal axes)
Unit cell	a= 5.3160 Å c= 7.1500 Å
I/Ic	1.38
Calc. density	2.674 g/cm³
Reference	Mellini M., Zanazzi P. F., "Effects of pressure on the structure of lizardite-1TSample: at P = 12.5 kbar", European Journal of Mineralogy **1**, 13-19 (1989)

D: Goethite (11.8 %)*

Formula sum	Fe O2
Entry number	96-901-5697
Figure-of-Merit (FoM)	0.668008*
Total number of peaks	187
Peaks in range	37
Peaks matched	16
Intensity scale factor	0.32
2theta correction	-0.043°
Space group	P b n m
Crystal system	orthorhombic
Unit cell	a= 4.6188 Å b= 9.9528 Å c= 3.0236 Å
I/Ic	3.17
Calc. density	4.198 g/cm³
Reference	Hazemann J.-L., Bérar J. F., Manceau A., "Rietveld studies of the aluminium-iron substitution in synthetic goethite", Materials Science Forum **79-82**, 821-826 (1991)

E: Montmorillonite (2.2 %)

Formula sum	Al2 Ca0.5 O12 Si4
Entry number	96-900-2780
Figure-of-Merit (FoM)	0.000000
Total number of peaks	92
Peaks in range	92
Peaks matched	31
Intensity scale factor	0.33
Space group	P 1
Crystal system	triclinic (anorthic)
Unit cell	a= 5.1800 Å b= 8.9800 Å c= 15.0000 Å α= 90.000° β= 90.000 ° γ= 90.000 °
I/Ic	17.33
Calc. density	1.801 g/cm³
Reference	Viani A., Gualtieri A., Artioli G., "The nature of disorder in montmorillonite by simulation of X-ray powderpatterns Note: Structural simulation model", American Mineralogist **87**, 966-975 (2002)

(*)2theta values have been shifted internally for the calculation of the amounts, the intensity scaling factors as well as the figure-of-merit (FoM), due to the active search-match option 'Automatic zero point adaption'.

Candidates

Name	*Formula*	*Entry No.*	*FoM*
	Ga16 Se33 Zn4	96-410-6294	0.7196
aluminum phosphate	Al O4 P	96-201-0796	0.7145
	H78.6 Na12.6 O86 P10 Pd15.4	96-700-2723	0.7121
) ((C5 H9 N H)2 (C H2)3)	Cd4 In16 S33	96-412-3975	0.7104

	C28 H183 Cu8 K4 N28 Na7 Nb54 O184	96-712-9691	0.7077
	C76 H179 N10 O60 Sb W18	96-450-0754	0.7075
	C60 Bi10 Br40 O25	96-713-0614	0.7052
	C32 H19 Ag12 F50 O29.5	96-411-5643	0.7020
	C132 H42 F80 Fe Mn12 O50	96-432-0646	0.6961
	Cl2 Cs3 Fe H36 K4 O95 Si2 Ta6 W18	96-722-6912	0.6942
Tridymite	O2 Si	96-901-3394	0.6910
	C120 Cl8 Mn4 N7 Ni O70 Si2 W18	96-703-5027	0.6891
	C18 Cl17 Cs3 N6 O61 Ti12	96-412-6915	0.6886
	C102 H227 Mo17 N9 O62 V3	96-700-3207	0.6886
(Zn4 In16 S33) ((C5 H9 N H)2 (C H2)3)	In16 S33 Zn4	96-412-3976	0.6877
(Co4 In16 S33) ((C5 H9 N H)2 (C H2)3)	Co4 In16 S33	96-412-3977	0.6873
	C120 Cl8 Cu Mn4 N7 O70 Si2 W18	96-703-5028	0.6872
	C12 O7 P2 Zn	96-431-1830	0.6870
	C120 Cl8 Co Mn4 N7 O70 Si2 W18	96-703-5026	0.6861
	Al1.55 Na1.55 O4 Si0.45	96-200-2896	0.6834
MOL-3CdS	C158 H138 Cd17 N4 S32	96-411-1893	0.6821
	C48 H84 Br24 Cr12 O110 Si W12	96-400-1632	0.6808
	C52 B6 Co F3 N7 O2	96-723-4123	0.6784
	C116 Ag2 Cr Lu2 Mn4 N14 O78 Si2 W18	96-712-0260	0.6778
	C118 Cl6 Mn5 N7 O70 Si2 W18	96-703-5024	0.6773
	C77 H190.2 Cu5 Ge0 In30 N11 O7.1 S53	96-722-8736	0.6750
	C258 H579 N17 O156 Si4 Ti8 W40	96-110-1220	0.6748
	C48 H96 Al21 Na21 O216 Si75	96-150-7214	0.6731
	C20 H9 Ag8 F18 N3 O12	96-411-5641	0.6716
	C124 Cl12 Cu4 Fe N7 O72 Si2 W18	96-434-6914	0.6710
COV-3CdS-BPy	C166 H138 Cd17 N2 S30	96-410-0573	0.6709
	C12 H94 Cu3 Ge K2 N12 Na4 Nb12 O65 V2	96-451-0028	0.6674
	C156 H134 Br4 Cd17 N2 S28	96-723-3663	0.6638
	Cs4 H62 K7 Na5 Nb23 O108 V5	96-712-7393	0.6636
	C324 H270 Cd33 S60	96-410-9637	0.6611
	C3 Cs2 K0.5 O68 P2 W18	96-156-1589	0.6609
	C10 H10 Co3 F2 N2 O8 P2	96-431-0851	0.6608
	C120 As24 O99 U10	96-433-5132	0.6596
	C8 H136 Fe6 N4 Na14 O184 Se6 W34	96-711-5857	0.6593
	C35 H11 Ag11 F45 N3 O19	96-411-5644	0.6581
	C12 Ga O5	96-770-3817	0.6568
	C347.64 H811.16 In60 N57.94 Se118.97	96-770-1506	0.6563
LiNaU20P12	Li6 Na18 O188 P12 S U20	96-434-5367	0.6549
LiNaU20P6	Li Na18 O162 P6 S U20	96-434-5366	0.6542
	C102 Ge N9 O36 W10	96-710-8167	0.6538
Au36	C120 H216 Au36 S24	96-151-4182	0.6533
	C144 Cu6 O42 P3	96-155-6348	0.6486
Na20 (Al20 Si76 O192)	Al20 Na20 O192 Si76	96-152-7028	0.6479
(C6 H12 (N H2)2)2 Zn Ga7 (H P O4)2 (P O4)6 (O H) F4 (H2 O)3	C12 H41 F4 Ga7 N4 O36 P8 Zn	96-152-6075	0.6475
	C64 H144 N4 O40 Si W12	96-431-9533	0.6469
	C96 N6 O36 Si W10	96-432-9779	0.6453

Pigment Green 7,Hostaperm Green GNX,Solid solution of CuPcCl16 (main component),CuPcHCl15, CuPcH2Cl14, CuPcH3Cl13 and CuPcH4Cl12.Average composition Cu C32 N8 H1.2 Cl14.8 ***and 78 others...***	C32 Cl16 Cu N8	96-210-8857	0.6451

Search-Match

Settings

Reference database used	COD-Inorg 2023.12.05
Automatic zeropoint adaptation	Yes
Downgrade entries with low scaling factors	Yes
Minimum figure-of-merit (FoM)	0.60
2theta window for peak corr.	0.30 deg.
Minimum rel. int. for peak corr.	0
Parameter/influence 2theta	0.50
Parameter/influence intensities	0.50
Parameter multiple/single phase(s)	0.50

Criteria for entries added by user

Reference:

Entry number: 96-901-5697;96-900-4995;96-900-8298;96-900-2780

Peak List

No.	*2theta [°]*	*d [Å]*	*I/I0 (peak height)*	*Counts (peak area)*	*FWHM*	*Matched*
1	5.59	15.7969	275.13	11.78	0.2800	
2	5.91	14.9423	310.76	32.32	0.6800	E
3	6.49	13.6082	156.68	6.71	0.2800	
4	6.85	12.8938	100.55	4.31	0.2800	
5	12.45	7.1039	279.97	18.84	0.4400	C
6	18.91	4.6891	215.04	11.84	0.3600	B
7	19.59	4.5279	194.03	5.93	0.2000	B
8	19.85	4.4692	268.85	27.96	0.6800	E
9	20.45	4.3394	202.04	59.32	1.9200	B,E
10	21.09	4.2091	364.39	57.95	1.0400	A,D
11	21.43	4.1431	201.83	24.69	0.8000	B
12	25.15	3.5381	345.05	19.00	0.3600	B,C
13	26.83	3.3202	1000.00	48.94	0.3200	A,B,E
14	28.49	3.1304	246.51	9.05	0.2400	B
15	28.79	3.0985	285.98	14.00	0.3200	B
16	31.29	2.8564	145.99	6.25	0.2800	E
17	33.29	2.6892	185.73	15.91	0.5600	D
18	34.79	2.5766	231.03	18.37	0.5200	B,D,E
19	35.25	2.5440	171.14	39.78	1.5200	D,E
20	35.95	2.4961	201.12	81.20	2.6400	B,C,D,E
21	36.83	2.4384	476.23	49.52	0.6800	A,B,D,E
22	39.77	2.2647	96.87	6.52	0.4400	A,B
23	40.07	2.2484	108.52	13.94	0.8400	D,E
24	40.41	2.2303	87.13	3.52	0.2639	A,B,E
25	41.19	2.1898	86.34	14.03	1.0627	B,C,D,E
26	42.75	2.1135	105.37	2.98	0.1849	A,B,C
27	50.39	1.8095	100.64	3.69	0.2400	A,B,D
28	53.29	1.7177	244.54	10.47	0.2800	B,D
29	53.67	1.7064	168.87	35.12	1.3600	B
30	58.97	1.5650	118.49	5.80	0.3200	B,C,D,E
31	59.21	1.5593	97.97	5.39	0.3600	B,D
32	60.21	1.5357	97.29	4.17	0.2800	A,B,C
33	61.43	1.5081	170.96	24.05	0.9200	B,D
34	63.63	1.4612	99.76	3.66	0.2400	B,E
35	64.97	1.4342	53.10	7.60	0.9365	B,C,E
36	68.57	1.3675	64.64	1.84	0.1659	A,B,C,D

Integrated Profile Areas

Based on calculated profile

Profile area	***Counts***	***Amount***
Overall diffraction profile	81885	100.00%
Background radiation	49258	60.16%
Diffraction peaks	32627	39.84%
Peak area belonging to selected phases	20362	24.87%
Peak area of phase A (Talc)	*6693*	*8.17%*
Peak area of phase B (Silicon oxide Quartz low)	*4352*	*5.31%*
Peak area of phase C (Montmorillonite)	*1680*	*2.05%*
Peak area of phase D (Lizardite)	*2273*	*2.78%*
hase E (Goethite)	*5363*	*6.55%*
eak area	12265	14.98%

Peak Residuals

Peak data	Counts	Amount
Overall peak intensity	706	100.00%
Peak intensity belonging to selected phases	469	66.35%
Unidentified peak intensity	238	33.65%

Diffraction Pattern Graphics